International Journal of Nanomedicine

Dovepress

open access to scientific and medical research

Open Access Full Text Article

ORIGINAL RESEARCH

MMP-2 Responsive Peptide Hydrogel-Based Nanoplatform for Multimodal Tumor Therapy

Qing Zhang[1,*], Wenjun Hu[1,*], Mingxue Guo[1], Xinyu Zhang[1], Qin Zhang[1], Fengqi Peng[1], Liwen Yan[1], Zucheng Hu[1], Jakkree Tangthianchaichana[2], Yan Shen[3], Haiyan Hu[4], Shouying Du[1], Yang Lu[1]

[1]School of Chinese Pharmacy, Beijing University of Chinese Medicine, Beijing, 102488, People's Republic of China; [2]Chulabhorn International College of Medicine, Thammasat University, Pathum Thani, 12120, Thailand; [3]School of Pharmacy, China Pharmaceutical University, Nanjing, 210009, People's Republic of China; [4]School of Pharmacy, Beijing Health Vocational College, Beijing, 101100, People's Republic of China

*These authors contributed equally to this work

Correspondence: Haiyan Hu, School of Pharmacy, Beijing Health Vocational College, Beijing, 101100, People's Republic of China, Email yxyhhy@163.com; Yang Lu, School of Chinese Pharmacy, Beijing University of Chinese Medicine, Beijing, 102488, People's Republic of China, Email luyang@bucm.edu.cn

Introduction: Responsive drug delivery systems hold great promise for tumor treatment as they focus on therapeutic agents directly, thus minimizing systemic toxicities and drug leakage. In this study, we covalently bound a matrix metalloproteinases-2 (MMP-2) enzyme-sensitive peptide to a tissue-penetrating peptide to rationally design a MMP-2 responsive multifunctional peptide hydrogel platform (aP/IR@FMKB) for cancer photothermal-chemo-immunotherapy. The constructed aP/IR@FMKB with bufalin (BF) loaded in trimethyl chitosan nanoparticles (TB NPs), photothermal agent IR820, and immune checkpoint inhibitor aPD-L1 by self-assembly could be dissociated in the presence of MMP-2 enzyme, triggering content release.

Methods: TB NPs, IR820, and aPD-L1 were encapsulated by intermolecular self-assembly and enzyme-sensitive nanogels (aP/IR@FMKB) were constructed. The in vitro cytotoxicity of the blank gels and their ability to induce immunogenic cell death (ICD) in aP/IR@FMKB were evaluated using 4T1 cells. The promotion of deep tumor penetration and enzyme responsiveness was analyzed using a 3D cell model. The retention and antitumor activity at the tumor sites were examined using the primary tumor model. To assess the antitumor effect of aP/IR@FMKB induced by the immune response and its mechanism of action, recurrent tumor and distal tumor models were constructed.

Results: This hydrogel system demonstrated exceptional photothermal performance and displayed prolonged local retention. Furthermore, the induction of ICD through IR820 and TB NPs sensitized the PD-L1 blockade, resulting in a remarkable 3.5-fold and 5.2-fold increase in the frequency of intratumor-infiltrating $CD8^+$ T-cells in the primary tumor and distal tumor, respectively. Additionally, this system demonstrated remarkable efficacy in suppressing primary, distal, and recurrent tumors, underscoring its potential as a highly potent therapeutic strategy.

Conclusion: This innovative design of the responsive hydrogel can effectively modulate the tumor immune microenvironment while also demonstrating sensitivity to the PD-1/PD-L1 blockade. This significant finding highlights the promising potential of this hydrogel in the field of multimodal tumor therapy.

Keywords: responsive drug delivery systems, peptide hydrogels, immunogenic cell death, PD-1/PD-L1 blockade

Introduction

Cancer, a highly lethal disease worldwide, exerts a profound impact on the quality of life of patients. In order to develop effective cancer therapies, nations have made substantial investments in terms of human, materials, and financial resources.[1] Currently, chemotherapy has been extensively employed in the clinic, demonstrating significant advancements in restraining tumor proliferation and extending patient survival.[2,3] The advent of photothermal therapy and immunotherapy has further revolutionized the field, exhibiting remarkable anticancer efficacy in numerous studies.[4–8] However, numerous clinical investigations have revealed that the physiological barriers inherent to tumors, such as dense extracellular matrix and elevated tumor interstitial pressure, severely impede the deep penetration of drug delivery

Received: 24 July 2023
Accepted: 25 December 2023
Published: 3 January 2024

systems at the tumor site, thereby compromising the desired antitumor effect.[9,10] Due to the intricate immune microenvironment, the self-renewal and differentiation of cancer stem cells, and aberrant alterations in signaling pathways implicated in tumor cell or immune cell proliferation, tumors are prone to develop resistance to monotherapy, leading to tumor recurrence and treatment failure.[11] Consequently, multimodal cancer treatment has emerged as the optimal approach. The rapid advancements in nanodrug delivery systems offer promising prospects for achieving a breakthrough in tumor treatment when combined with multimodal therapy, owing to their high efficiency, stability, and precise targeting capabilities.[12–14] Therefore, the design of nano carriers, based on the aforementioned challenges in tumor treatment, which judiciously integrate diverse treatment modalities and facilitate the synergistic effects of nanodrug delivery systems, holds the key to effectively inhibiting tumor growth in situ and simultaneously preventing tumor recurrence, thereby enhancing the overall efficacy of tumor treatment.

In recent years, responsive drug delivery systems have garnered significant attention from scientists and scholars due to their notable advantages over non-responsive administration. These advantages include the reduction of off-target adverse events, increased drug accumulation at disease sites, and improved permeability to target cells within biomembranes.[15,16] The mechanism of action of immune checkpoint inhibitors (ICIs) lies in blocking the immune inhibitory receptors on tumor cells, such as programmed death-1 (PD-1), cytotoxic T lymphocyte-associated antigen-4 (CTLA-4), and lymphocyte-activation gene-3 (LAG-3), thereby enhancing the cytotoxicity and proliferative capacity of tumor infiltrating lymphocytes (TILs). Among them, monoclonal antibodies targeting PD-1, PD-L1 and CTLA-4 have been proven effective in various types of tumors. Although anti-PD-1 and anti-PD-L1 antibodies have received approval from the US Food and Drug Administration (FDA) for clinical use, clinical responses to ICIs have been somewhat constrained. Based on the knowledge of PD-L1 expression not only in tumor cells but also in other normal cells or tissues, such as vascular endothelial cells and the eye, etc, there is a need for responsive drug delivery systems to effectively implement PD-1/PD-L1 blockade cancer immunotherapy. The responsive systems help prevent non-specific binding of aPD-L1 antibodies to non-target tissues, thus enhancing the therapeutic effect of aPD-L1 by specifically promoting T-cell activation.[17]

In a previous study,[18] bufalin (BF) was incorporated into TMC-based nanoparticles to develop TB NPs with the aim of achieving enhanced tumor penetration. However, the efficacy of TB NPs in suppressing tumor recurrence is hindered by the intricate immunosuppressive microenvironment within tumors, which poses challenges in harnessing the individual immunogenic cell death (ICD) effects induced by TB NPs. Therefore, as shown in Scheme 1, based on the merits of multimodal therapy, the matrix metalloproteinase-2 (MMP-2) enzyme sensitive peptide PLGLAG was covalently bound to the tumor-penetrable peptide CRGDK, and TB nanoparticles, photosensitizer IR820 and PD-L1 antibodies were loaded through self-assembly between polypeptides to construct a TB/aPD-L1/IR820 based peptide hydrogel nanoplatform (aP/IR@FMKB) with MMP-2 response and tumor tissue penetration capability. This platform effectively modulated the immune microenvironment by inducing the ICD effect and blocking the PD-1/PD-L1 pathway within the tumor. The aP/IR@FMKB hydrogel nanoplatform exhibited prolonged local retention, allowing targeted delivery and release of therapeutic agents specifically within the tumor interior, where the MMP-2 enzyme is highly expressed. This localized delivery strategy resulted in effective tumor inhibition and immune response activation. Furthermore, when combined with laser irradiation, the hydrogel triggered ICD, sensitized cells to PD-1/PD-L1 blockade, and facilitated infiltration of intratumoral cytotoxic T lymphocytes (CTLs). The multimodal therapy offered by the aP/IR@FMKB nanoplatform demonstrated its efficacy in tumor inhibition and held significant promise for broader applications in cancer theranostics.

Materials and Methods

MMP-2 sensitive tumor penetrable Fmoc-KPLGLAGCRGDK (FMK) peptide and tumor-penetrable Fmoc-KCRGDK (FK) peptide were obtained from GL Biochem (Shanghai), Ltd. (Shanghai, China) through solid-phase synthesis. Bufalin and sulforhodamine B (SRB) were purchased from Yuanye Biotechnology Co., Ltd. (Shanghai, China). TB NPs at 100 μg/mL of bufalin were prepared following our previously described method.[18] The MMP-2 enzyme, new indocyanine green (IR820), was purchased from Sigma-Aldrich (Shanghai, China). In vivo mAb anti-mouse PD-L1 (catalog number BE0101) was obtained from Bio X Cell (USA). IgG was purchased from Dalian Meilun Biotechnology Co., Ltd. (Dalian, China) and ELISA kits for the IgG assay were purchased from J&L Biological (Shanghai, China). 4', 6-diamidino-2-phenylindole

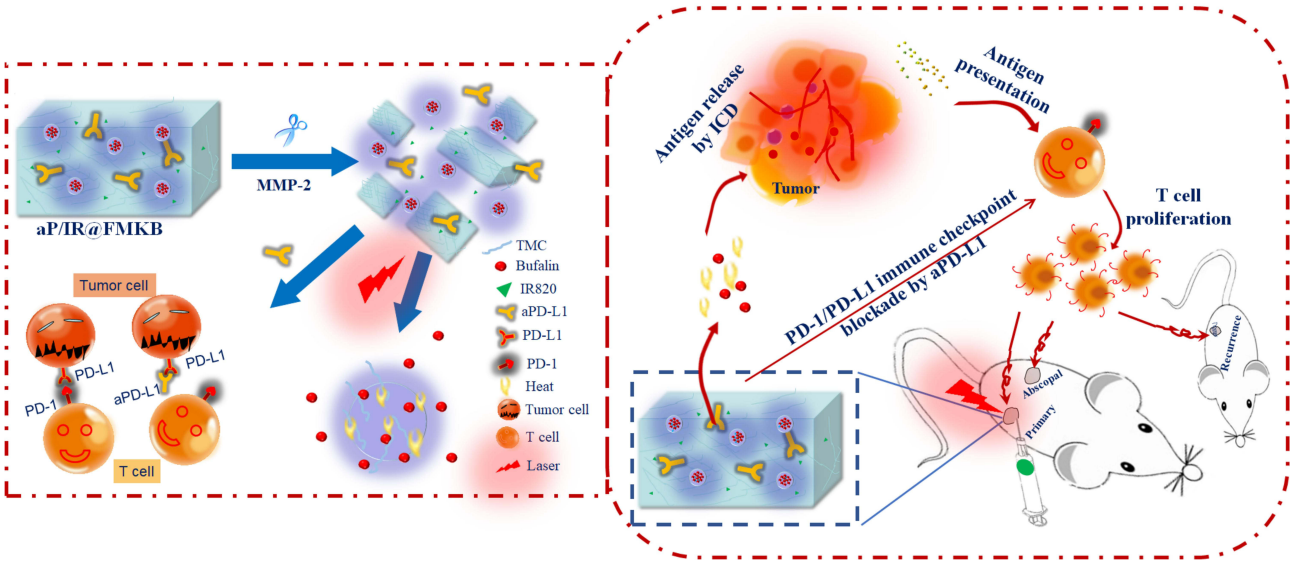

Scheme 1 Schematic illustration of drug release and tumor inhibition of the intratumoral injected aP/IR@FMKB hydrogel.

(DAPI) and an ATP assay kit (S0026) were supplied by the Beyotime Institute of Biotechnology (Jiangsu, China). The ELISA kit for high mobility group box 1 (HMGB1) was purchased from Solarbio (SEKM-0145) and Collagenase IV, DNase, and hyaluronidase (HAase) were purchased from Yeasen (Shanghai, China). Fluorochrome-marked anti-mouse monoclonal antibodies (CD4, CD8, CD3, CD62L, CD44, Foxp3, Ki67, TNF-α, and IFN-γ) and FVD780 were purchased from eBioscience (San Diego, CA). All other reagents (AR grade) were used as received without further purification.

NIH 3T3 mouse embryonic fibroblast cells and 4T1 murine breast tumor cells were purchased from the National Infrastructure of Cell Resources (Beijing, China), maintained in RPMI medium containing fetal bovine serum (FBS, 10%), penicillin (100 U/mL), and streptomycin (100 mg/mL), and incubated in a 5% CO_2 atmosphere at 37°C. All cell culture reagents were purchased from Gibco (USA).

Female BALB/c mice (4- to 6-weeks-old) were provided by the Vital River Laboratory Animal Technology Co., Ltd. (Beijing, China). Animals were acclimated to the animal care facility for a few days prior to building the breast cancer model by subcutaneous injection of 4T1 cells into the flanks of mice at 1.0×10^6 cells per mouse. Animals were raised under pathogen-free conditions. Animal care was performed in compliance with the guidelines of the Ministry of Science and Technology of China (2006) and the related ethical regulations of Beijing University of Chinese Medicine. The protocol of the current study was approved by the Ethical Committee (25-3-2019) for Laboratory Animals of Beijing University of Chinese Medicine (No: BUCM-4-2019032502-1072). All experimental procedures were designed to minimize animal suffering and the number of animals used.

The Formation of the MMP-2 Responsive Multifunctional Peptide Hydrogel

TB NPs were synthesized according to a previously reported protocol.[18] A blank hydrogel was fabricated from 10 mg FMK and 5 mg FK in 1 mL distilled water at 70°C. After being vortexed for 10s, the blank hydrogel was stirred with 0.5 mg IR820, TB NPs with 0.1 mg bufalin, and 1 mg aPD-L1 for 5 min at room temperature to prepare the MMP-2 responsive multifunctional peptide hydrogel.

The Morphology of Hydrogels

The appearance of the blank hydrogel and aP/IR@FMKB was captured using a camera. The structure of aP/IR@FMKB was observed by transmission electron microscopy (FE-TEM; JEM-2100, Japan). The surface morphology of freeze-dried aP/IR@FMKB was examined using scanning electron microscopy (SEM, Hitachi S4800). In addition, MMP-2

sensitivity of the aP/IR@FMKB hydrogel was tested using TEM. After incubation with the MMP-2 enzyme in purified water for 30 min, we observed structural changes with TEM, in contrast to the hydrogel without the MMP-2 enzyme.

The Rheology Analysis of Hydrogels

Rheological analysis of the blank hydrogel and aP/IR@FMKB hydrogel was performed using a HAAKE MARS 60 rheometer (Germany). The storage modulus (G') and loss modulus (G') were measured within a frequency sweep range of 0.1–100 rad/s. The strain was set at 1.0% and the temperature was 25°C. Thixotropy was investigated by vortexing for 5 s, and the state of the hydrogel was observed after stewing for 1 h. We further pulled the aP/IR@FMKB hydrogel using a syringe, injected it back into a vital state, and observed the state of the hydrogel.

The Photothermal Property in vitro of Hydrogels

For in vitro evaluation of the photothermal properties of water, free IR820 and aP/IR@FMKB hydrogels were added to 1.5 mL EP tubes and irradiated with an 808 nm NIR laser at a power density of 0.5 W/cm^2 for 4 min. Temperature changes and thermal images were recorded using a high-performance infrared imaging system (Ax5 camera; FLIR Systems Inc., USA).

The Release Behavior Study of Hydrogels

For in vitro release studies of each content from the hydrogel, a hydrogel loaded with TB NPs, IgG, and IR820 was added into the transwell chamber and immersed in the released media on 24-well plates, including PBS (pH 7.4) and 500 ng/mL MMP-2 in PBS (pH 7.4). The samples in 24-well plates were incubated on a shaker at 37°C, and all the media of the sample were collected for further analysis at predetermined time intervals. The same volume of media was then added to a 24-well plate. Each sample in the laser group was irradiated with an 808 nm laser after 2 h. The concentrations of bufalin and IgG in all the sample media were measured using high-performance liquid chromatography (HPLC) and a mouse IgG ELISA kit (JL12948), respectively.

The Biosafety Evaluation of Blank Hydrogel

The blank hydrogel (200 μL) was extracted using DMEM and RPMI 1640 medium to prepare the stock solution. NIH 3T3 and 4T1 cells were seeded in 96-well plates and incubated overnight in various media. The blank hydrogel solution was then added to each well at a concentration range of 0.1–3 mg/mL and incubated for 24 h. After incubation, cell viability was analyzed using the sulforhodamine B (SRB) assay.

The Distribution in Multicellular Spheroids of Hydrogels

Tumor penetration capacity of aP/IR@FMKB hydrogel using 4T1-derived multicellular spheroids (MCSs) was detected. Briefly, 100 μL of 2.0% (w/v) fresh agarose was added to the bottom of a 24-well plate, and 4T1 cells (2×10^3/well) were seeded into pre-coated 24-well plates and incubated for 7 days to form spheroids. These spheroids were divided into three groups: aP/IR@FMKB hydrogel, aP/IR@FMKB hydrogel + MMP-2, and aP/IR@FMKB hydrogel + MMP-2 + Laser. The aP/IR@FMKB hydrogel (100 μL) was pretreated with RPMI 1640 medium, and 100 μL of the aP/IR@FMKB hydrogel was pretreated with 500 ng/mL MMP-2 in RPMI 1640 medium. Afterwards, the culture medium of the spheroids was replaced with pretreated RPMI 1640 medium and 500 ng/mL MMP-2 in RPMI 1640 medium. MCSs were incubated for 8 h to achieve penetration. The laser group was treated with an 808 nm NIR laser at a power density of 0.5 W/cm for 3 min after 2 h of administration, and then incubated for 6 h. the intracellular uptake and distribution of aP/IR@FMKB hydrogel was then observed using confocal laser scanning microscope (CLSM) examination (Leica, Germany).

The Induction of Immunogenic Cell Death Effect of Hydrogels

Given the ICD effects of bufalin and laser irradiation, the ability of the aP/IR@FMKB hydrogel to induce calreticulin (CRT) exposure, ATP secretion, and HMGB1 efflux was measured in 4T1 cancer cells. For CRT detection, immunofluorescence was performed using CLSM. Briefly, 4T1 cells (4×10^3/well) were seeded in a 24-

well plate containing round coverslips and incubated overnight. Each group of aP/IR@FMKB + MMP-2 + L, aP/IR@FMKB, TB NPs, Free aP/IR/BF + L, and bufalin (BF) were added to each well at 2 μg/mL BF, 10 μg/mL IR820, and 20 μg/mL aPD-L1; cells without any treatment were used as the control group. After 12 h, the culture medium was replaced with fresh RPMI 1640. The laser group was irradiated with an 808 nm NIR laser at a power density of 0.5 W/cm^2 for 2 min, and then incubated for 4 h. Afterwards, the cells were washed three times with cold PBS and fixed in 4% paraformaldehyde for 20 min, washed twice with cold PBS and blocked up with 5% FBS for 30 min, then incubated with specific primary antibody of anti-CRT (Abcam, ab2907, 1:200) after washing again twice in cold PBS. After 30 min, the cells were washed twice and incubated with a FITC-conjugated monoclonal secondary antibody (Abcam, ab6717, 1:1000). Finally, the nuclei were stained with DAPI and visualized using a confocal CLSM. The secretion of ATP from each group was determined using an ATP assay kit, whereas the efflux of HMGB1 from each treatment group was tested using an ELISA assay kit. The laser group was irradiated after 12 h of incubation and then incubated for 12 h. The cell culture supernatant was collected and centrifuged at 1000 × g for 10 min. The amount of ATP or HMGB1 in the supernatant was analyzed using an assay kit, according to the manufacturer's instructions.

The in vivo Photothermal Effect of Hydrogels

4T1 cells (1 × 10^6) in 100 μL PBS were inoculated into the third mammary pad of each mouse (BALB/c, female, 6 weeks old, 18–20 g) to build a 4T1 primary tumor model. When the tumor grew to 300 mm^3, 100 μL of aP/IR@FMKB hydrogel or free IR820 was injected directly into the tumor site. After 12 h, the tumor area was irradiated with an 808 nm laser, and the temperature changes and thermal images were recorded.

The Retention and Penetration in vivo of Hydrogels

Hydrogels can achieve long retention at the injection site and produce a marked effect with drug release constantly.[19] Therefore, we evaluated the intratumor retention of the aP/IR@FMKB hydrogel in the 4T1 tumor model. For the controls, free IR820 solution was injected into the tumor area. IR820 fluorescence was captured using an IVIS Spectrum system (MIIS, Multi-function In vivo Imaging System) at different intervals. To determine the penetration of the hydrogel under laser irradiation, we used water-soluble fluorescent dye-SRB to substitute the PD-L1 antibody and prepared a peptide hydrogel (abr. SRB/IR@FMKB), using the same method. One hundred microliters of each group was injected slowly in the tumor site, including the free SRB/IR820 solution (abr. Free SRB/IR820), SRB/IR820 + laser, SRB/IR@FMKB, and SRB/IR@FMKB + laser groups. The laser group was irradiated with an 808 nm laser at a density of 0.5 W/cm^2 for 3 min after 12 h. Afterwards, the tumors were collected and sectioned in a cryostat (Leica, Germany) and fixed in 4% paraformaldehyde for 20 min, washed twice with cold PBS and stained with DAPI for 30 min, then the fluorescence signals were observed in CLSM.

The Inhibition of 4T1 Primary Tumor of Hydrogels

To examine the tumor inhibition capacity of the aP/IR@FMKB hydrogel, we established a 4T1 primary tumor model by subcutaneously injecting 100 μL of PBS suspended in 4T1 cells (1 × 10^6) on the left flank of each female BALB/c mouse. When the tumor volume reached approximately 100 mm^3, the mice were randomly divided into eight groups and intratumors were administered 100 μL of PBS, free aP/IR/BF + L, TB NPs, FMKB, aP@FMKB, aP/IR@FMKB, IR@FMKB + L, aP/IR@FMKB, and aP/IR@FMKB + L (BF, 100 μg/mL; IR820, 500 μg/mL; aPD-L1, 1.0 mg/mL). Each mouse in the laser group was irradiated with an 808 nm laser at 0.5 W/cm^2 for 3 min post 12 h of intratumor injection. The body weight of the mice was recorded and plotted, the tumor size was documented using a digital caliper, and the volume was calculated using the formula: length × width^2 × 0.5. Mice were necropsied at the end of the experiment and tumor tissues were weighed and photographed to directly evaluate the efficacy of tumor growth suppression. The major organs (ie, the heart, liver, spleen, and kidney) were collected for further analysis using H&E staining.

The Inhibition of 4T1 Recurrent Tumor of Hydrogels

To study the inhibition of recurrent tumors, we constructed 4T1 recurrent tumors. Briefly, 4T1 tumor cells (1×10^6) were subcutaneously injected into the left flank of the BALB/c mice. On day 7 after tumor inoculation, most primary tumors (200 mm^3) were resected. When the tumor had relapsed to 100 mm^3, the 4T1 recurrent tumor model was built successfully. Mice in each group were injected as described above. Recurrent tumor size and body weight were monitored every 3 days. Finally, the survival time of the remaining mice in each group was recorded until day 60 after the first administration, and survival curves were mapped.

The Inhibition of 4T1 Distal Tumor of Hydrogels

To estimate the abscopal effect of the aP/IR @FMKB-based combination on 4T1 distal tumors, we built a dual-tumor model. Briefly, while inoculating the primary tumor in the left flank with 1×10^6 4T1 tumor cells, distal tumors were established simultaneously by inoculating 2×10^5 4T1 tumor cells in the right flank. After the primary tumor volume reached 100 mm^3, the mice in the eight groups were treated as described above, and the distal tumor size of each mouse was documented.

The in vivo Analysis of Different Treatments of Immune Cells

To evaluate the immune response induced by aP/IR@FMKB hydrogel-based therapy, the primary tumors, spleens, and distal tumors were collected after different treatments and washed with PBS to remove residual bloodstains and adherent tissue or skin. For the extraction and isolation of lymphocytes, the tumors were cut and digested with various enzymes at 37°C for 1 h, including collagenase (175 U/mL^1), hyaluronidase (100 U/mL), and deoxyribonuclease (30 U/mL). After digestion was complete, serum-containing RPMI 1640 was added to terminate digestion and ground with a syringe piston. Suspensions containing tumor-infiltrating lymphocytes (TILs) were filtered through 75 μm sterile filters and isolated using lymphocytic cell separating medium. The obtained TILs were stained with anti-CD3-BV421, anti-CD4-BV786, and anti-CD-BV605 antibodies according to standard instructions to examine the content of $CD8^+$ T-cells in the tumors using flow cytometry. Next, to study the functions and proliferation of TILs, TILs were fixed and permeabilized using a FoxP3/Transcription Factor Staining Buffer Kit (eBioscience) and stained with an anti-Ki67-PerCP-Cy5.5 antibody. We then added a leukocyte activation cocktail, with BD GolgiPlug™, to TILs to elicit a primary cytokine response, fixed and permeabilized with a Fixation/Permeabilization Kit, and then stained with TNF-α-Alexa Fluor 647 and IFN-γ-FITC antibodies before investigation by flow cytometry. Treg cells were stained with anti-CD4-BV786 and anti-CD25-APC antibodies, fixed, permeabilized using a FoxP3/Transcription Factor Staining Buffer Kit, and stained with an anti-FoxP3-PE antibody. According to the standard protocols, anti-CD3-BV421, anti-CD44-PerCP-Cy5.5, and anti-CD62L-PE antibodies were used for T_{EM} cell staining.

Statistical Analysis

All data are presented as the mean ± SD. The flow data were analyzed using a BD FACSDivaTM, and the other data were plotted using OriginPro 8.5. Student's *t*-test was used to analyze and compare differences between groups. Statistical significance is listed as follows: $*P<0.05$, $**P<0.01$.

Results and Discussion

In order to prepare the aP/IR@FMKB hydrogel for tumor drug delivery, we synthesized two peptide sequences: Fmoc-KCRGDK (FK), which possessed a tumor-penetrable peptide sequence, and Fmoc-KPLGLAGCRGDK (FMK), which incorporated a tumor-penetrable peptide sequence sensitive to MMP-2 (Figure S1 and S2). The inclusion of the CendR motif (CRGDK) within these peptide sequences facilitated enhanced penetration into tumor tissue by binding to neuropilin-1 (Nrp-1), a transmembrane receptor glycoprotein that was known to be overexpressed in tumor vessels and cells.[20] Furthermore, the presence of two 9-fluorenylmethyloxycarbonyl (Fmoc) groups within the peptide sequences promoted self-assembly and hydrogel formation through the π–π stacking of their aromatic groups and hydrophobic interactions.[21] Moreover, to enhance the specificity of drug release in the tumor region, a MMP-2-labile peptide

PLGLAG was incorporated within the FMK sequence. This peptide sequence could be cleaved by the highly expressed MMP-2 enzyme in the tumor microenvironment.[22,23] In order to assess the cleavability of the MMP-2-responsive sequence, we conducted an incubation experiment, where FMK was exposed to the MMP-2 enzyme. The resulting samples were then https://www.dovepress.com/get_supplementary_file.php?f=#####.pdfanalyzed using HPLC and mass spectrometry. Comparative analysis of the FMK spectra, as depicted in Figure S2B and Figure S2C, revealed the absence of the m/z 830.45 peak in the FMK mass spectra and the peak eluting at a retention time of 10.94 min in the FMK chromatogram (Figure S3). These findings suggested that FMK can indeed be disrupted under MMP-2 enzyme conditions. However, it was previously reported that direct insertion of MMP-2 sensitive hexapeptides could negatively impact the assembly process and result in a non-gellable peptide, as it disrupted the beta sheet assembly, which was essential for peptide gellability.[24] Hence, to overcome this limitation, we opted to mix FK with FMK in an appropriate mass ratio to facilitate successful gel formation.

The visual appearance of the aP/IR@FMKB hydrogel was captured using a camera. Figure S4A showcased a blank hydrogel (@FMK) that was ivory in color and exhibited a semitransparent nature, devoid of any encapsulated content. In contrast, Figure S4B depicted the aP/IR@FMKB hydrogel, which displayed a light green semitransparent appearance. The formation process of aP/IR@FMKB was documented using TEM. As illustrated in Figure S4C–Figure S4E, the FK and FMK mixed peptides initially formed micelles when placed in purified water. Over time, these micelles underwent a gradual transformation, evolving into assembled nanofibers, and eventually culminating in the formation of hydrogels (Figure 1A). The 3D structural morphology of the hydrogels was further confirmed by scanning electron microscopy (SEM) analysis, as depicted in Figure 1B.

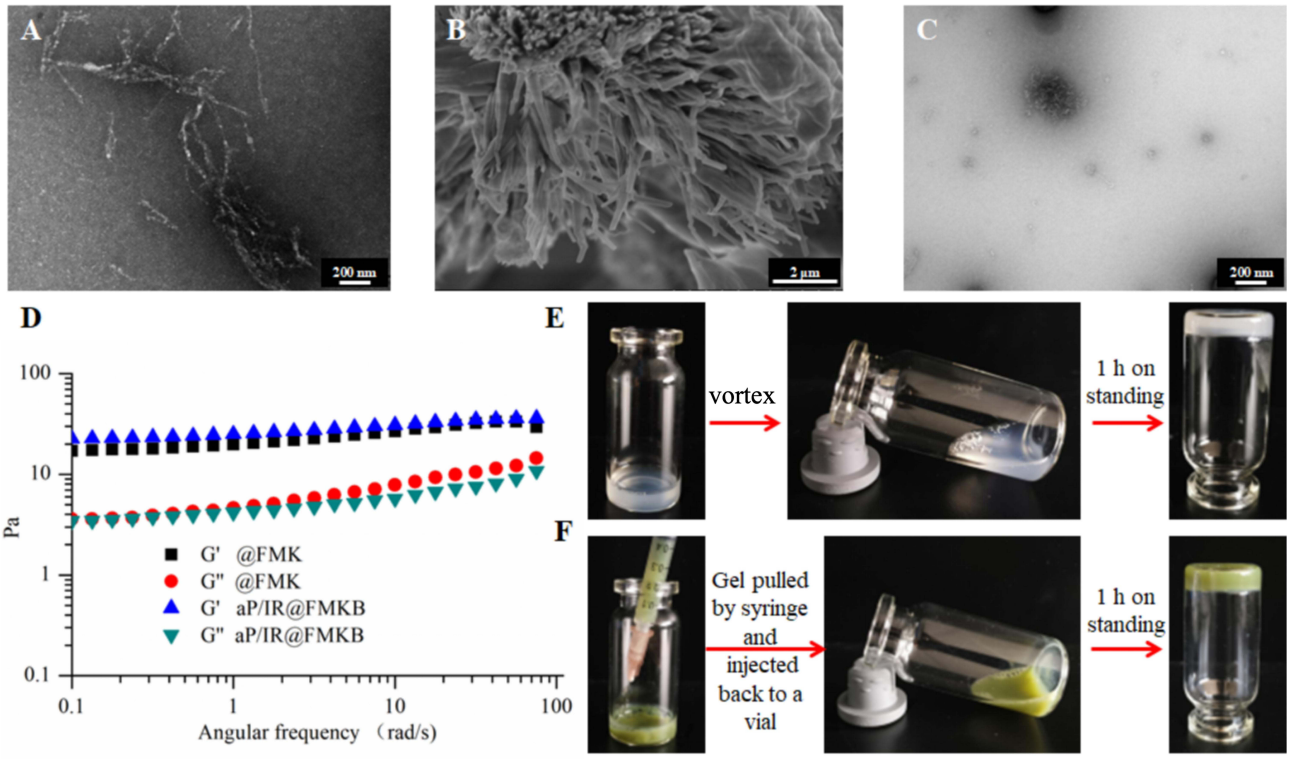

Figure 1 Characterization of aP/IR@FMKB for multimodal tumor therapy.
Notes: (**A**) TEM (Scale bar = 200 nm), and (**B**) SEM (Scale bar = 2 μm) images of aP/IR@FMKB hydrogel. (**C**) TEM (Scale bar, 200 nm) examination of aP/IR@FMKB hydrogel after incubating with MMP-2 enzyme. (**D**) Frequency-dependent (strain 1%) rheological properties of blank hydrogel (@FMK) and aP/IR@FMKB hydrogel. (**E**) Illustration of the thixotropic, and (**F**) injectable nature of the hydrogel.
Abbreviations: TEM, transmission electron microscopy; SEM, Scanning electron microscopy; MMP-2, matrix metalloproteinases-2.

In order to validate the susceptibility of aP/IR@FMKB hydrogels to degradation by MMP-2 enzyme, we conducted a 30 min incubation of the hydrogels with MMP-2 enzyme, followed by observation using TEM. As depicted in Figure 1C, the obtained image clearly illustrated the disruption and absence of the 3D structure, as anticipated. This enzymatic degradation held great promise for facilitating the targeted release of encapsulated contents at the tumor site.

Next, the viscoelastic properties of aP/IR@FMKB and blank @FMK were explored using a rheometer. As illustrated in Figure 1D, the storage modulus G' (the amount of stress required to shear the elastic component of the gel by a unit strain, meaning elasticity) and the loss modulus G' (the amount of stress required to shear the viscous component of the gel by a unit strain, meaning viscosity) of both hydrogels remained relatively stable as the frequency increased. Moreover, the value of G' was consistently higher than that of G', indicating the gel-like nature of the hydrogel.

In order to assess the thixotropic behavior of aP/IR@FMKB, we examined the changes in fluidity when the hydrogel was subjected to stress and when the stress was subsequently removed. As depicted in Figure 1E, upon application of vortexing, the hydrogel underwent liquefaction and reverted back to its gel state once the stress was alleviated. These findings not only demonstrated the thixotropic nature of the hydrogel, which enabled the incorporation of biological components and facilitated their direct injection into target sites (Figure 1F), but also established its role as a reservoir for localized retention and controlled release of therapeutic agents.

Our objective was to develop an aP/IR@FMKB hydrogel loaded with IR820 to achieve an exceptional photothermal effect, capable of inducing tumor photothermal ablation and triggering immunogenic cell death (ICD). This, in turn, would facilitate the recruitment of immune cells and mitigate the risk of postoperative breast cancer recurrence. Subsequently, the photothermal effect of aP/IR@FMKB was assessed under 808 nm laser irradiation at a power density of 0.5 W/cm^2 for 240 s, with water solution serving as the control. Both aP/IR@FMKB and free IR820 exhibited a progressive increase in temperature over time, while the aqueous solution displayed no significant change (Figure 2A).

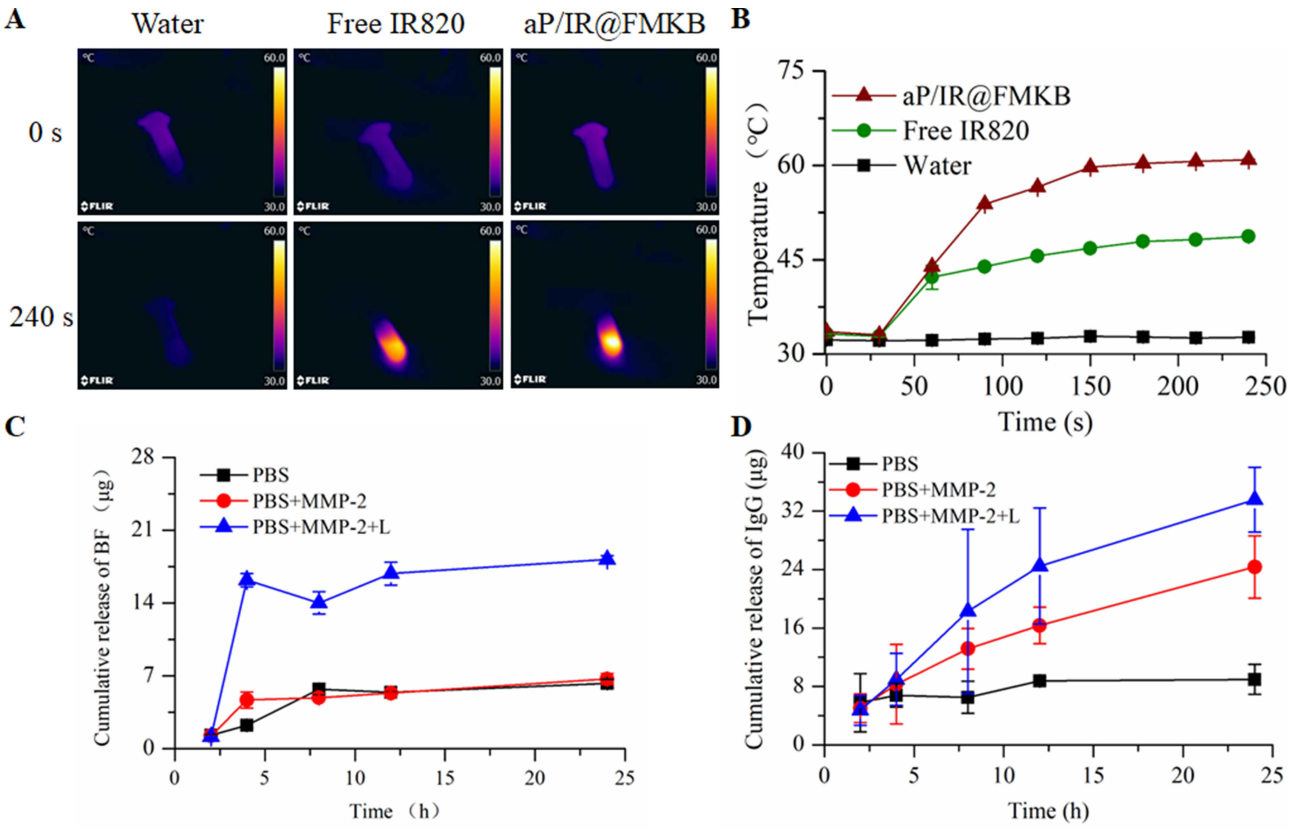

Figure 2 Comparison of the photothermal efficacy of aP/IR@FMKB hydrogel.
Notes: (**A**) The typical thermal images upon 808 nm laser irradiation. (**B**) Time-dependent temperature change profiles during NIR laser irradiation at 0.5 W/cm^2. The cumulative release curve of BF (**C**) and PD-L1 (**D**) from hydrogel in different medium.
Abbreviations: NIR, near infrared; BF, bufalin.

Notably, the temperature of aP/IR@FMKB eventually reached approximately 60°C, indicating an enhanced photothermal performance in the gel state (Figure 2B).

Given the exceptional photothermal performance of this drug delivery system and its incorporation of a MMP-2 sensitive peptide, we proceeded to evaluate the release behavior of agents triggered by laser irradiation and MMP-2 enzyme in the aP/IR@FMKB hydrogel. As illustrated in Figure 2C, the release of bufalin in the presence of MMP-2 enzyme in PBS was comparable to that in PBS medium alone. This observation suggested that MMP-2 enzyme had no discernible impact on the release behavior of bufalin within the hydrogel. This could be attributed to the fact that bufalin in the hydrogel was encapsulated within trimethyl chitosan nanoparticles, which did not exhibit enzyme sensitivity. Consequently, it was necessary for the nanoparticles to be released from the hydrogel first, followed by a subsequent gradual release of bufalin from the nanoparticles. However, after laser irradiation, the release rate of bufalin within the hydrogel increased significantly by 2.6 times compared to that in PBS medium.

Subsequently, we conducted an evaluation of the release behavior of aPD-L1 in various media. To assess the release profiles in vitro, IgG was employed as a substitute for aPD-L1 and co-loaded with IR820 and TB NPs into the aP/IR@FMKB hydrogel.[25] As depicted in Figure 2D, the release of IgG from the hydrogel, indicated by the black line, exhibited a sluggish release pattern in PBS medium, with only approximately 9 μg released within 24 h. However, when the hydrogel was incubated with MMP-2 enzyme, the release of IgG increased significantly. After 24 h, the amount of IgG released was approximately 2.7 times higher compared to that in PBS medium. Subsequently, we investigated the release behavior of IgG under 808 nm laser irradiation after 2 h. The results demonstrated that laser irradiation, in conjunction with MMP-2 enzyme, facilitated the release of IgG, with approximately 9 μg released after 4 h. Moreover, the amount of IgG released within 24 h was approximately 4 times higher than that in PBS medium, indicating a substantial increase in the release rate. These findings strongly suggested that aP/IR@FMKB hydrogel was sensitive to MMP-2 enzyme and that laser irradiation can effectively promote the release of loaded agents from the hydrogel, thereby establishing aP/IR@FMKB as a highly promising drug reservoir.

In order to assess the biocompatibility of blank@FMK for safe drug delivery, we conducted sulforhodamine B (SRB) assays using various cell lines. As depicted in Figure S5, the results demonstrated that treatment with different concentrations of blank@FMK resulted in more than 90% cell viability in 4T1, NIH 3T3, and HC11 cells. These findings provided strong evidence for the low cytotoxicity and exceptional cytocompatibility of blank@FMK.

The limited distribution of therapeutics within tumors poses a significant challenge in drug delivery design.[26,27] To assess the tumor penetration capability of the aP/IR@FMKB hydrogel, we conducted experiments using multicellular spheroids (MCSs) derived from 4T1 cells. MCSs, as 3D tumor models, closely mimic the tumor microenvironment and are widely utilized for analyzing tumor biological behavior and evaluating cancer therapeutics.[28] In this study, we prepared MCSs and treated them with 500 ng/mL of MMP-2 enzyme to simulate the enzyme-rich microenvironment prior to aP/IR@FMKB incubation. As shown in Figure 3A, the red signal representing IR820 was primarily observed in the outer layer of MCSs when cultured in medium without MMP-2 enzyme. However, pre-incubation with MMP-2 significantly enhanced the penetration of aP/IR@FMKB into the tumor spheroids. Upon exposure to 808 nm laser irradiation, intense red signals were observed throughout the entire spheroid when MMP-2 enzyme was present, suggesting that the MMP-2 sensitivity of aP/IR@FMKB combined with laser irradiation could effectively loosen the dense tumor stroma and enhance the penetration of therapeutic agents into the tumor. These findings demonstrated that the inclusion of the tumor penetration peptide motif (CRGDK) and the application of laser irradiation confer the MMP-2 responsive aP/IR@FMKB hydrogel with a robust photothermal effect and remarkable tumor penetration capability. Consequently, the aP/IR@FMKB hydrogel held great promise as a drug delivery system in cancer treatment.

Several recent clinical trials and studies have indicated that ICD can enhance the efficacy of PD-1/PD-L1 blockade, suggesting a potential therapeutic approach.[29] To investigate the ICD effect induced by aP/IR@FMKB, we examined the translocation of CRT, secretion of ATP, and nuclear activity of HMGB1 in 4T1 tumor cells. As shown in Figure 3B, the green fluorescence representing CRT was clearly observed in the BF, Free aP/IR/BF+L, TB NPs, aP/IR@FMKB, and aP/IR@FMKB+L groups, in contrast to the PBS group. Moreover, both the free aP/IR/BF+L and aP/IR@FMKB+L groups exhibited stronger fluorescence intensities under laser irradiation. During the process of ICD, ATP serves as a "find-me" signal to enhance the antitumor immune response.[30] The release of ATP in the 4T1 cell culture supernatant was

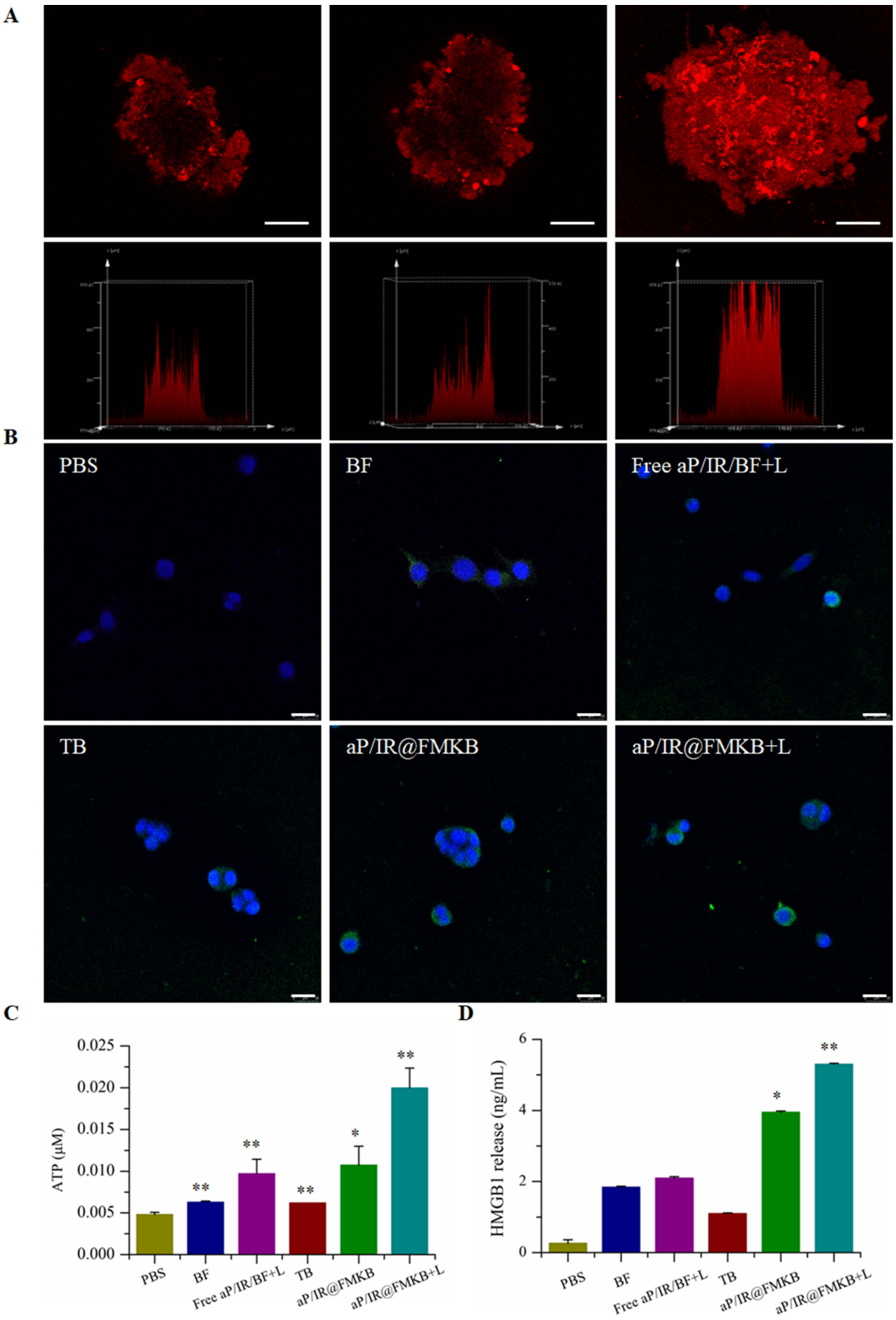

Figure 3 In vitro evaluation of aP/IR@FMKB in 4T1 breast cancer cells.

Notes: (**A**) Tumor penetration capability of aP/IR@FMKB in MCSs model in (left) RPMI 1640 medium; (media) RPMI 1640 medium with 500 ng/mL MMP-2 enzyme; (right) RPMI 1640 medium with 500 ng/mL MMP-2 enzyme upon laser irradiation. (**B**) Impact of aP/IR@FMKB on upregulating CRT exposure (green signals) of 4T1 cells by CLSM, scale bar = 75 μm; Impact of aP/IR@FMKB on (**C**) ATP and (**D**) HMGB1 release from 4T1 cells (n = 3), **P*<0.05, ***P*<0.01.

Abbreviations: MCS, multicellular spheroid; MMP-2, matrix metalloproteinases-2; CRT, calreticulin; CLSM, Confocal laser scanning microscopy; ATP, adenosine triphosphate; HMGB1, high-mobility group protein.

illustrated in Figure 3C. Compared to the PBS group, the other treatment groups showed varying degrees of increased ATP secretion. Notably, under laser irradiation, the aP/IR@FMKB group exhibited significantly higher ATP secretion compared to the aP/IR@FMKB group alone, with a 1.86-fold increase, 3.18-fold increase, and 2.06-fold increase compared to the aP/IR@FMKB alone, BF, and Free aP/IR/BF+L groups, respectively. Under physiological conditions, HMGB1 was predominantly localized in the nucleus, resulting in its almost undetectable levels in the PBS group. However, treatment with aP/IR@FMKB and laser irradiation led to a significant release of HMGB1, with levels reaching 20.11-fold higher than that of the PBS group, 1.34-fold higher than that of the aP/IR@FMKB group alone, and 2.88-fold higher than that of the BF group (Figure 3D). These findings collectively demonstrated that the combination of aP/IR@FMKB and laser irradiation effectively induced ICD effects in 4T1 cells. Afterwards, the tumor cells could be more readily recognized by antigen-presenting cells, leading to enhanced lymphocyte infiltration and increased sensitivity to PD-1/PD-L1 blockade.

Subsequently, we assessed the photothermal effect using the 4T1 breast cancer model (Figure 4A). Upon laser irradiation, the temperature of both the free IR820 solution and aP/IR@FMKB gradually increased over time. After 120 s, the aP/IR@FMKB hydrogel elevated the intratumoral temperature by 18.5°C. In contrast, animals treated with the free IR820 solution exhibited a significantly lower temperature increase of 10.6°C (Figure 4B). Overall, the formation of the hydrogel enhanced the photothermal performance of IR820 compared to the solution rapidly dispersing at the tumor site.

To evaluate the capacity of the hydrogel to prolong the retention duration of therapeutics within tumors, model mice were monitored at various time points after intratumoral injection using a fluorescence in vivo imaging system (IVIS). The fluorescence intensity of free IR820 was relatively weak, suggesting rapid dispersion and clearance of the drug. In contrast, the fluorescence intensity of IR820 encapsulated in the aP/IR@FMKB group remained consistently high throughout the monitoring period (Figure S6). This prolonged retention of IR820 indicated that the aP/IR@FMKB hydrogel effectively concentrated the drug at the tumor site and extended the duration of action as a reservoir.

To gain further insights into the distribution of aP/IR@FMKB within the tumor, tumor tissue sections were examined using confocal imaging, with and without laser irradiation. In order to observe the fluorescent signal at different excitation/emission wavelengths, a favorable water-soluble dye-SRB was used as a substitute for aPD-L1.[31] The SRB was encapsulated together with IR820 in the aP/IR@FMKB hydrogel. The confocal imaging analysis, as shown in Figure S7, clearly demonstrated the prominent signal distribution and strong colocalization of SRB and IR820 in the aP/IR@FMKB groups, both with and without laser irradiation. In contrast, the signal was barely detected in the free SRB/IR820 group, indicating the successful formation and retention of the peptide hydrogel in the tumor regions. This achievement enabled optimal tissue penetration and specific targeting of tumor cells through the CRGDK motif. Furthermore, the fluorescence signal distribution in the laser groups, whether using the aP/IR@FMKB hydrogel or free SRB/IR820, was stronger compared to the non-laser groups. This observation suggested that laser irradiation can enhance tissue penetration and drug diffusion,

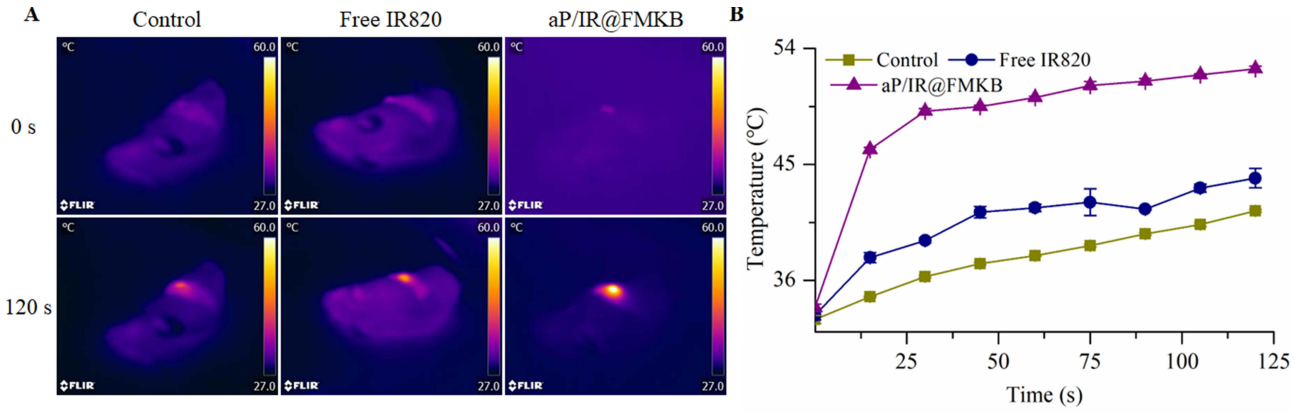

Figure 4 Photothermal effect of aP/IR@FMKB in vivo.
Notes: (**A**) The typical thermal images upon NIR laser irradiation. (**B**) Time-dependent temperature change profiles during 808 nm laser irradiation.
Abbreviation: NIR, near infrared.

thereby making the aP/IR@FMKB hydrogel a promising platform for localized drug delivery and multimodal treatment mediated by aPD-L1.

The exceptional photothermal performance, sustained laser effect, MMP-2 enzyme-triggered content release behavior, and induction of a superior ICD effect observed with the aP/IR@FMKB hydrogel prompted us to further investigate its multimodal tumor inhibition. The experimental schedule for the in vivo experiments was outlined in Figure 5A. Capitalizing on the responsive drug delivery capabilities of the hydrogel, we evaluated the significant antitumor activity of the aP/IR@FMKB hydrogel in the 4T1 tumor-bearing BALB/c mouse model. As depicted in Figure 5C and Figure 5E, on the 4th day (day 12) following the completion of triple administration, the tumor growth inhibition rates were 71% and 93% with free aP/IR/BF and IR@FMKB groups, respectively, in conjunction with 808 nm laser irradiation. Upon the introduction of the PD-L1 antibody, primary tumors in the aP/IR@FMKB group were completely eliminated. However, over time, treatment with TB NPs had a negligible effect on tumor growth, similar to that observed in the PBS group. Moreover, upon 808 nm laser irradiation, uncontrolled tumor growth was observed in the free aP/IR/BF group, while the IR@FMKB group exhibited some degree of inhibition. This could be attributed to the presence of an immunosuppressive microenvironment that could undermine the sustainability of the immune response. Notably, the primary tumor inhibition rate in the aP/IR@FMKB + laser group exceeded 90%, resulting in complete tumor regression in five out of six mice (Figure S8A). Throughout the study, we assessed the biocompatibility of the hydrogel-based combination therapy by monitoring the weight changes of the mice in each group (Figure S8B) and conducting hematoxylin and eosin (H&E) staining of the tissue (Figure S9). Importantly, no significant weight loss was observed during the entire experimental period, and no visible signs of inflammatory response or tissue injury were observed in the heart, liver, spleen, and kidney upon H&E staining. These findings indicated the excellent biocompatibility of our hydrogel system.

Given the remarkable antitumor activity observed with the hydrogel-based therapy, we conducted an estimation of recurrent tumor inhibition (Figure 5B). The results depicted in Figures 5D and 5F demonstrated a delayed growth of recurrent tumors in the IR@FMKB + laser group. However, a more pronounced inhibition rate and a substantial survival benefit were observed in the aP/IR@FMKB + laser group, with complete disappearance of recurrent tumors in half of the mice. Importantly, no significant weight loss was observed during the course of the study (Figure 5G). These findings indicated that the local recurrent tumors were effectively suppressed by the aP/IR@FMKB hydrogel-based combination therapy.

It has been previously reported that ICD can sensitize immune checkpoint blockade, and the combination of ICD with a PD-L1 blocking antibody can recruit and activate cytotoxic T lymphocytes (CTLs). This activation of CTLs enabled direct recognition of tumor cells, leading to tumor eradication and the development of long-lasting immune protection.[29,32] Given that the aP/IR@FMKB hydrogel incorporated a MMP-2 responsive peptide and a tissue penetration motif, this hydrogel was expected to effectively deliver a PD-L1 antibody for blocking PD-1/PD-L1 interaction and bufalin for inducing ICD upon 808 nm laser irradiation. This combined approach created a more favorable tumor immune microenvironment for multimodal cancer therapy. Furthermore, the results of in vivo tumor growth inhibition experiments also demonstrated the enhanced antitumor properties of this approach. To gain a deeper understanding of the underlying mechanism behind the enhanced antitumor activity, we further investigated the proportion, proliferation, and activation of intratumoral CTL infiltration with different treatments using flow cytometry (gated on $CD3^+$ T-cells). On the 4th day after the completion of triple administration, tumor tissues were excised, and lymphocytes were collected to analyze $CD8^+$ ($CD3^+CD4^-CD8^+$) T-cells (Figure 6A). The TB NPs and FMKB groups exhibited a slight increase in $CD8^+$ T-cell infiltration compared to the PBS group, with no significant difference observed between the two groups. This suggested that the ICD effect induced by bufalin can promote the recruitment and infiltration of lymphocytes, and that the gelation matrix used in the study did not possess immunogenicity or affect lymphocyte infiltration. Following the introduction of the PD-L1 antibody and the photosensitizer IR820, there was almost no difference in tumor infiltration of $CD8^+$ T-cells between the aP@FMKB and aP/IR@FMKB groups. However, both groups demonstrated a 2-fold increase in $CD8^+$ T-cell infiltration compared to the PBS group. This indicated that IR820 alone did not affect $CD8^+$ T-cell

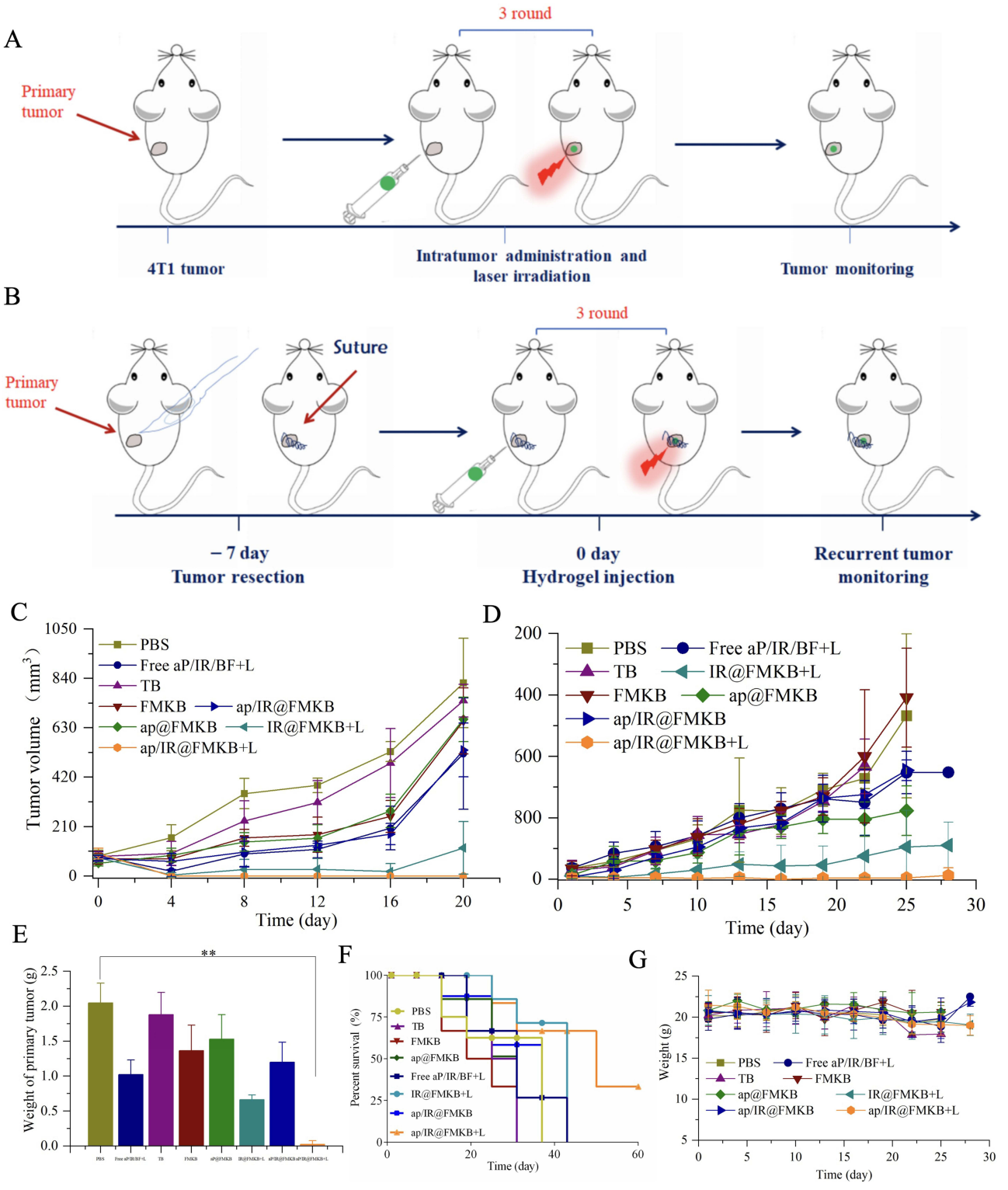

Figure 5 aP/IR@FMKB hydrogel-performed multimodal tumor therapy in primary and recurrent tumor model.

Notes: Therapeutic schedule in primary (**A**) and recurrent (**B**) tumor model. Average tumor growth curves of the primary (**C**) and recurrent (**D**) tumors receiving different treatments (laser irradiation for 3 min at photodensity of 0.5 W/cm^2). Data were presented as mean ± SD (n = 6). (**E**) The inhibition of primary tumor growth by various formulations, $^{**}P<0.01$. (**F**) Survival rate of the 4T1 recurrent tumor. The death time of all the mice in different groups: PBS, day 37. TB NPs, day 31. FMKB, day 31. aP@FMKB, day 31. Free aP/IR/BF + L, day 43. IR@FMKB + L, day 43. aP/IR@FMKB, day 37. aP/IR@FMKB + L, day 60. (**G**) The body weight alteration of each group.

https://doi.org/10.2147/IJN.S432112 DovePress

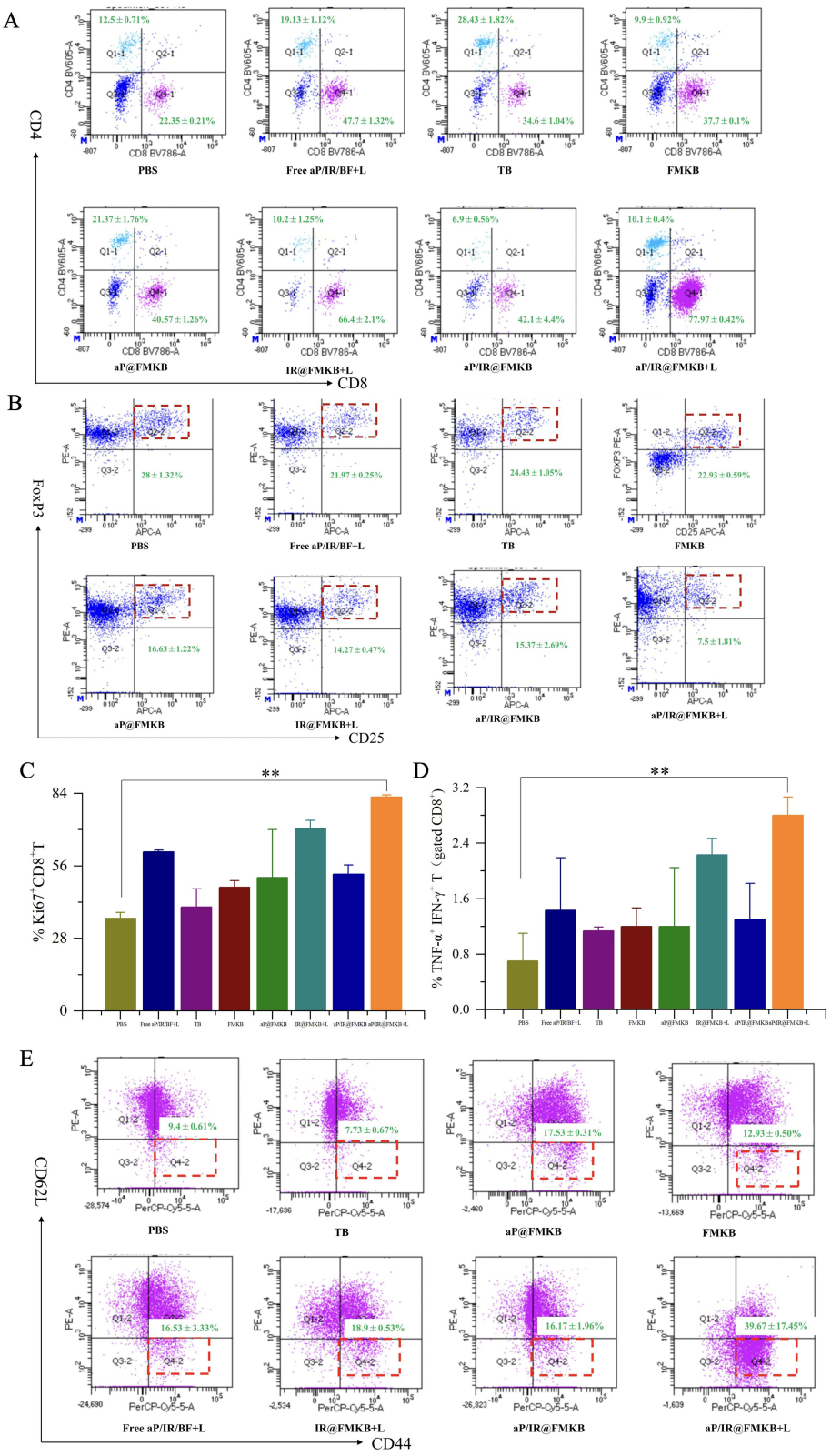

Figure 6 aP/IR@FMKB induced immune response in vivo.

Notes: (**A**) Flow cytometric examination of the intratumoral infiltration of $CD4^+$ and $CD8^+$ T-cells (gated on $CD3^+$ T-cells). Data were presented as mean ± SD (n = 3). (**B**) The frequency of Treg ($CD25^+CD4^+FOXP3^+$) in the primary tumors after different treatments examined day 12 after the start of treatment. Data were presented as mean ± SD (n = 3). (**C**) The proliferation activity of $CD8^+$ T-cells in the primary tumor, $^{**}P<0.01$. (**D**) The frequency of TNF-α^+/IFN-γ^+ $CD8^+$ T-cells in the primary tumor, $^{**}P<0.01$. (**E**) Flow cytometry plots and proportions of effector memory T-cells in the spleen (gated on $CD8^+$ $CD11b^+$) on a recurrent tumor model.

Abbreviation: Treg, regulatory cells.

infiltration without laser irradiation, while the PD-L1 antibody effectively blocked the PD-1/PD-L1 interaction. The gelation of PD-L1 reduced off-site accumulation and improves stability. Moreover, the number of infiltrating $CD8^+$ T-cells significantly increased in the laser irradiation groups compared to the non-laser group. In particular, the aP/IR@FMKB + laser group exhibited a higher frequency of intratumor infiltrating $CD8^+$ T-cells, reaching 77.97 ± 0.42%, which was 3.5-fold higher than that observed in the PBS group. These findings highlighted the necessity of hydrogel formation encapsulated with the PD-L1 antibody, IR820, bufalin, and the induction of ICD through photothermal therapy (PTT) and chemotherapeutic drugs. This combination sensitized the PD-L1 antibody to checkpoint blockade, resulting in robust antitumor lymphocyte infiltration and immune response within the tumor microenvironment.

Regulatory T (Treg) cells have been widely recognized for their suppressive functions within the tumor immune microenvironment, which can contribute to tumor progression, recurrence, and poor prognosis by inhibiting antitumor immune responses.[33] In fact, Tregs are now considered a major obstacle in tumor treatment. Therefore, we utilized flow cytometry to measure the levels of $CD4^+$, $CD25^+$, and $Foxp3^+$ in Tregs on day 12 after treatment initiation (Figure 6B). The elevated levels of Tregs in the PBS group indicated that the 4T1 tumor itself exhibited significant immunosuppression. In contrast, the TB NPs and FMKB groups displayed slightly lower proportions of Tregs, suggesting that the ICD effect alone was insufficient to impact the immunosuppressive microenvironment. Notably, the introduction of the PD-L1 antibody greatly reduced Tregs in the aP@FMKB and aP/IR@FMKB groups, indicating that the combination of ICD effect and PD-1/PD-L1 interaction blockade was the most effective strategy for modulating the immunosuppressive microenvironment. Remarkably, the number of Tregs in the aP/IR@FMKB + laser group was 3.5-fold lower than that in the PBS group, illustrating that the aP/IR@FMKB-based multimodal approach, encompassing PD-L1 blockade, PTT, and ICD induction, effectively alleviated immunosuppression and elicited antitumor immunity.

To validate the proliferation of $CD8^+$ T-cells, we employed the Ki-67 antibody as an immunofluorescence staining marker.[34] The aP/IR@FMKB-based multimodal therapy prominently enhanced the proliferation of $CD8^+$ T-cells, as evidenced by 82.63% of Ki-67-positive cells among the $CD8^+$ T-cell population (Figure 6C). Moreover, this multimodal therapy also augmented the presence of tumor necrosis factor α (TNF-α) and interferon-γ (IFN-γ) dual-positive CTLs by 4.0-fold compared to the PBS group (Figure 6D). TNF-α and IFN-γ are crucial immune cytokines that play a pivotal role in immune system activation and CTL function, including the secretion of perforin and granzyme to eliminate tumor cells.[35] These findings collectively demonstrated that the aP/IR@FMKB-based multimodal therapy can enhance the proliferation and functionality of CTLs, thereby amplifying the immune response for effective tumor inhibition.

At the conclusion of the recurrent tumor inhibition study, we assessed the proportion of effector memory T-cells (T_{EM}; $CD3^+CD44^+CD62L^-$) in the spleen. As illustrated in Figure 6E, mice treated with aP/IR@FMKB + laser exhibited a significantly higher number of T_{EM} cells compared to the other groups. Correspondingly, the frequency of T_{EM} cells in the aP/IR@FMKB + laser group was 3.1 and 1.8 times greater than that in the PBS and free aP/IR/BF + laser groups, respectively. These findings suggested that the combination therapy can elicit a more robust immune memory response, leading to sustained therapeutic benefits and inhibition of tumor recurrence.

Subsequently, we sought to investigate whether the immune response elicited by aP/IR@FMKB-based multimodal therapy was sufficiently robust to induce an abscopal effect on untreated distal tumors. To establish the distal tumor model, 4T1 breast cancer cells were injected into both flanks of the mice, with only the primary tumors being subjected to treatment (Figure 7A). As depicted in Figures 7B and 7C, mice treated with aP/IR@FMKB + laser exhibited slower growth of distal tumors compared to the other groups. Furthermore, when compared to the aP/IR@FMKB + laser group, the free aP/IR/BF + laser group demonstrated limited effects on the distal tumors, indicating that the sustained release of therapeutic agents from the peptide hydrogel not only elicited an immune response in the primary tumor but also maintained an abscopal immune response.

To provide a more comprehensive understanding of the enhanced abscopal effect following multimodal therapy, we employed flow cytometry to assess the infiltration of $CD8^+$ CTLs and Tregs into tumors. The percentage of $CD8^+$ CTLs infiltrating the distal tumors in the aP/IR@FMKB + laser group was found to be 5.2

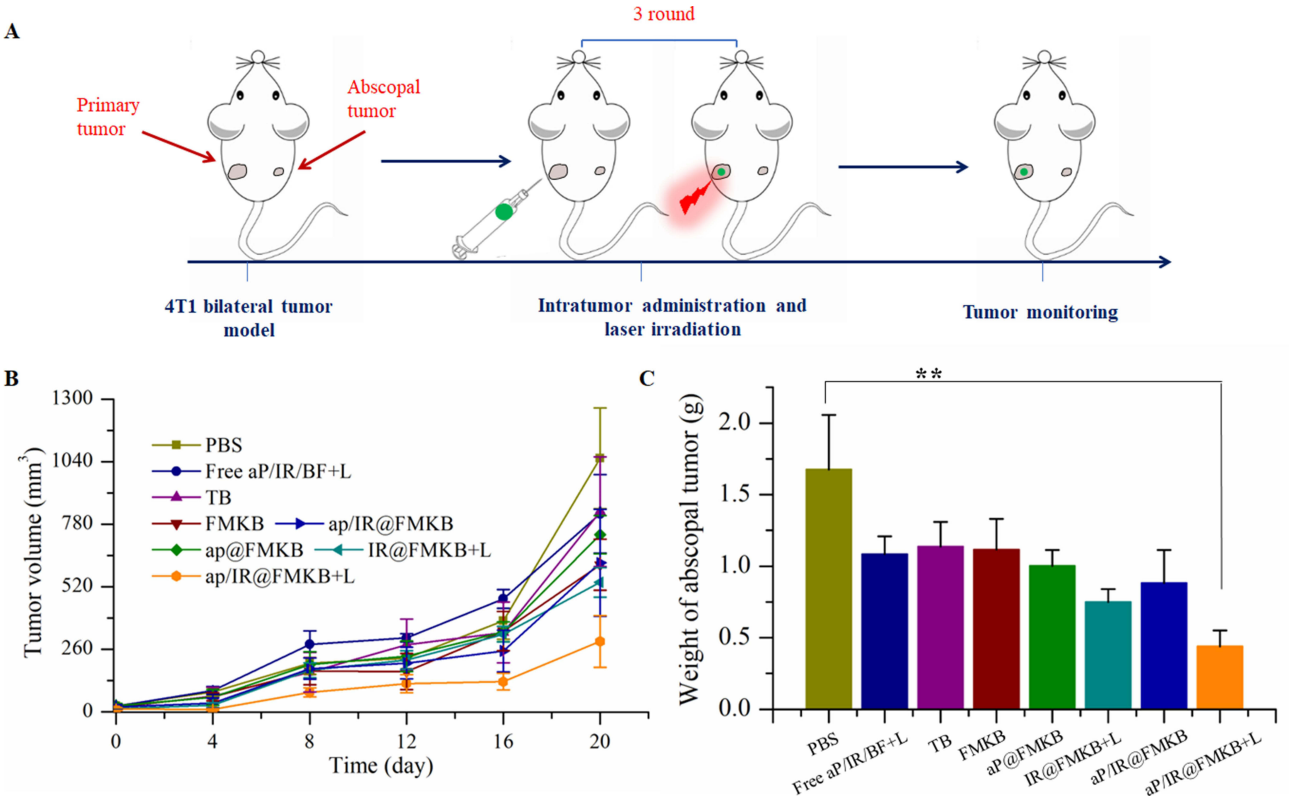

Figure 7 Abscopal effect of aP/IR@FMKB.
Notes: (**A**) Treatment schedule for aP/IR@FMKB mediated inhibition of distant tumor. (**B**) Distant tumor growth curves receiving different treatments. (**C**) The inhibition of distant tumor growth by various formulation, $^{**}P<0.01$.

and 1.5 times higher than that in the PBS and free aP/IR/BF + L groups, respectively (Figure 8A). Furthermore, a significant reduction in Tregs was observed in the distal tumors when the primary tumor was treated with the aP/IR@FMKB hydrogel and laser irradiation (Figure 8B). These findings provided compelling evidence that multimodal therapy modulated the tumor microenvironment and reversed immune tolerance in distal tumors.

Conclusion

Given the complexity of the immune microenvironment and the abnormal changes in signal pathways associated with cell proliferation in tumor cells or immune cells, tumors often develop tolerance to single therapies, leading to tumor recurrence and treatment failure.[36–38] To address this challenge, multimodal treatments that can maximize therapeutic efficacy by generating a cumulative response hold great promise for cancer therapy. In this study, we introduced an intelligent MMP-2 responsive hydrogel for local and deep tumor treatment. This hydrogel incorporated TB NPs, the photothermal agent IR820 and the immune checkpoint inhibitor aPD-L1, enabling multimodal tumor therapy.

In comparison to existing drug delivery systems, the aP/IR@FMKB designed in this study possesses several distinct advantages. Firstly, it incorporates multiple functions into a single system, taking into consideration the characteristics of tumor cells and the tumor microenvironment. Secondly, this design allows for the organic integration of the ICD effect and the blocking of the PD-1/PD-L1 signal pathway by loading bufalin, the photosensitizer, and immune checkpoint inhibitors. This integration provides valuable insights for the integration and optimization of local multi-mode antitumor effects. This intelligent MMP-2 responsive hydrogel specifically targets the breast tumor microenvironment and integrates three types of therapeutic agents within a single nanoplatform. This design enables the regulation of the tumor immune microenvironment and sensitizes the tumor to PD-1/PD-L1 blockade. These findings indicate a promising strategy for the development of responsive systems with multimodal tumor therapy.

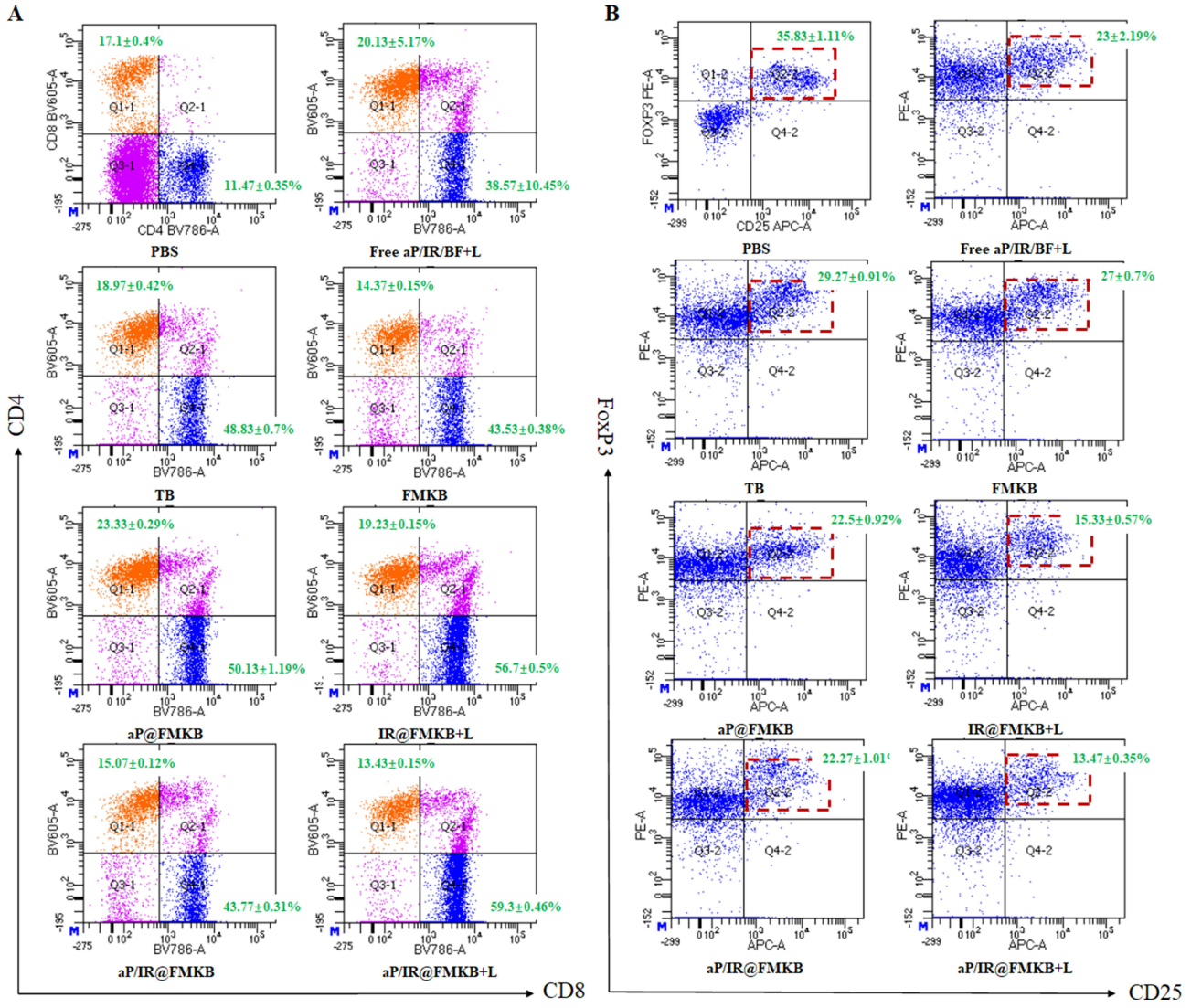

Figure 8 Abscopal effect prevention via immune response induced by aP/IR@FMKB.
Notes: Representative flow cytometry plots showing the proportions of tumor-infiltrating CTLs (**A**) and Treg (**B**) in distant 4T1 tumors. Data were presented as mean ± SD (n = 3).

Acknowledgments

This study was funded by the National Natural Science Foundation of China (no. 82173989).

Disclosure

All authors have no conflicts of interest for this work to disclose.

References

1. Adam F, Manju S, Dorothy L, et al. Access to cancer medicines deemed essential by oncologists in 82 countries: an international, cross-sectional survey. *Lancet Oncol*. 2021;22(10):1367–1377. doi:10.1016/S1470-2045(21)00463-0
2. Yi X, Zeng W, Wang C, et al. A step-by-step multiple stimuli-responsive metal-phenolic network prodrug nanoparticles for chemotherapy. *Nano Res*. 2021;15(2):1205–1212. doi:10.1007/s12274-021-3626-2
3. Lu Y, Aimetti AA, Langer R, et al. Bioresponsive materials. *Nature Rev Mater*. 2016;2(1):16075. doi:10.1038/natrevmats.2016.75
4. Tan T, Wang H, Cao H, et al. Deep tumor-penetrated nanocages improve accessibility to cancer stem cells for photothermal-chemotherapy of breast cancer metastasis. *Adv Sci*. 2018;5(12):1801012. doi:10.1002/advs.201801012
5. Jiang Y, Li J, Zhen X, et al. Dual-peak absorbing semiconducting copolymer nanoparticles for first and second near-infrared window photothermal therapy: a comparative study. *Ad. Mater*. 2018;30(14):e1705980. doi:10.1002/adma.201705980

6. Chen F, Zang Z, Chen Z, et al. Nanophotosensitizer-engineered Salmonella bacteria with hypoxia targeting and photothermal-assisted mutual bioaccumulation for solid tumor therapy. *Biomaterials*. 2019;214:119226. doi:10.1016/j.biomaterials.2019.119226
7. Sanmamed MF, Chen L. A paradigm shift in cancer immunotherapy: from enhancement to normalization. *Cell*. 2018;175(2):313–326. doi:10.1016/j.cell.2018.09.035
8. Yang Q, Peng J, Shi K, et al. Rationally designed peptide-conjugated gold/platinum nanosystem with active tumor-targeting for enhancing tumor photothermal-immunotherapy. *J Control Release*. 2019;308:29–43. doi:10.1016/j.jconrel.2019.06.031
9. Rosenblum D, Joshi N, Tao W, et al. Progress and challenges towards targeted delivery of cancer therapeutics. *Nat Commun*. 2018;9(1):1410. doi:10.1038/s41467-018-03705-y
10. Blanco E, Shen H, Ferrari M. Principles of nanoparticle design for overcoming biological barriers to drug delivery. *Nature Biotechnol*. 2015;33(9):941–951. doi:10.1038/nbt.3330
11. Binnewies M, Roberts EW, Kersten K, et al. Understanding the tumor immune microenvironment (TIME) for effective therapy. *Nature Med*. 2018;24(5):541–550. doi:10.1038/s41591-018-0014-x
12. Tian G, Zhang X, Gu Z, et al. Recent advances in up conversion nanoparticles-based multifunctional nanocomposites for combined cancer therapy. *Adv Mater*. 2015;27(47):7692–7712. doi:10.1002/adma.201503280
13. Li J, Zhang C, Gong S, et al. A nanoscale photothermal agent based on a metal-organic coordination polymer as a drug-loading framework for effective combination therapy. *Acta Biomater*. 2019;94:435–446. doi:10.1016/j.actbio.2019.06.014
14. Fan W, Yung B, Huang P, et al. Nanotechnology for multimodal synergistic cancer therapy. *Chem Rev*. 2017;117(22):13566–13638. doi:10.1021/acs.chemrev.7b00258
15. Singh A, Peppas NA. Hydrogels and scaffolds for immunomodulation. *Adv Mater*. 2014;26(38):6530–6541. doi:10.1002/adma.201402105
16. Wang F, Xu D, Su H, et al. Supramolecular prodrug hydrogelator as an immune booster for checkpoint blocker–based immunotherapy. *Sci Adv*. 2020;6:12.
17. Sharpe AH, Wherry EJ, Ahmed R, et al. The function of programmed cell death 1 and its ligands in regulating autoimmunity and infection. *Nat Immunol*. 2007;8(3):239–245. doi:10.1038/ni1443
18. Hu H, Qi Q, Dong Z, et al. Albumin coated trimethyl chitosan-based targeting delivery platform for photothermal/chemo-synergistic cancer therapy. *Carbohydr Polym*. 2020;241:116335. doi:10.1016/j.carbpol.2020.116335
19. George J, Hsu -C-C, Nguyen L, et al. Neural tissue engineering with structured hydrogels in CNS models and therapies. *Biotechnol Adv*. 2020;42:107370. doi:10.1016/j.biotechadv.2019.03.009
20. Liu Y, Zhang D, Qiao ZY, et al. A peptide-network weaved nanoplatform with tumor microenvironment responsiveness and deep tissue penetration capability for cancer therapy. *Adv Mater*. 2015;27(34):5034–5042. doi:10.1002/adma.201501502
21. Eskandari S, Guerin T, Toth I, et al. Recent advances in self-assembled peptides: implications for targeted drug delivery and vaccine engineering. *Adv Drug Delivery Rev*. 2017;110–111:169–187. doi:10.1016/j.addr.2016.06.013
22. Wang Y, Ye F, Liang Y, et al. Breast cancer brain metastasis: insight into molecular mechanisms and therapeutic strategies. *Br J Cancer*. 2021;125(8):1056–1067. doi:10.1038/s41416-021-01424-8
23. Cheng K, Ding Y, Zhao Y, et al. Sequentially responsive therapeutic peptide assembling nanoparticles for dual-targeted cancer immunotherapy. *Nano Lett*. 2018;18(5):3250–3258. doi:10.1021/acs.nanolett.8b01071
24. Chau Y, Luo Y, Cheung AC, et al. Incorporation of a matrix metalloproteinase-sensitive substrate into self-assembling peptides - a model for biofunctional scaffolds. *Biomaterials*. 2008;29(11):1713–1719. doi:10.1016/j.biomaterials.2007.11.046
25. Huang L, Li Y, Du Y, et al. Mild photothermal therapy potentiates anti-PD-L1 treatment for immunologically cold tumors via an all-in-one and all-in-control strategy. *Nat Commun*. 2019;10(1):4871. doi:10.1038/s41467-019-12771-9
26. Su YL, Hu SH. Functional nanoparticles for tumor penetration of therapeutics. *Pharmaceutics*. 2018;10(4):193. doi:10.3390/pharmaceutics10040193
27. Hung CC, Huang WC, Lin YW, et al. Active tumor permeation and uptake of surface charge-switchable theranostic nanoparticles for imaging-guided photothermal/chemo combinatorial therapy. *Theranostics*. 2017;7(3):559–560. doi:10.7150/thno.18728
28. Chau WK, Ip CK, Mak AS, et al. c-Kit mediates chemoresistance and tumor-initiating capacity of ovarian cancer cells through activation of Wnt/beta-catenin-ATP-binding cassette G2 signaling. *Oncogene*. 2013;32(22):2767–2781. doi:10.1038/onc.2012.290
29. Kepp O, Zitvogel L, Kroemer G. Clinical evidence that immunogenic cell death sensitizes to PD-1/PD-L1 blockade. *Oncoimmunology*. 2019;8(10):e1637188. doi:10.1080/2162402X.2019.1637188
30. Sun F, Cui L, Li T, et al. Oxaliplatin induces immunogenic cells death and enhances therapeutic efficacy of checkpoint inhibitor in a model of murine lung carcinoma. *J Recept Signal Transduct Res*. 2019;39(3):208–214. doi:10.1080/10799893.2019.1655050
31. Chaiyasan W, Srinivas SP, Niamprem P, et al. Penetration of hydrophilic sulforhodamine B across the porcine cornea ex-vivo. *Int J Appl Pharm*. 2018;10(6):94. doi:10.22159/ijap.2018v10i6.28505
32. Cerbelli B, Pernazza A, Botticelli A, et al. PD-L1 expression in TNBC: a predictive biomarker of response to neoadjuvant chemotherapy. *Biomed Res. Int.* 2017;2017:1750925. doi:10.1155/2017/1750925
33. Tanaka A, Sakaguchi S. Regulatory T cells in cancer immunotherapy. *Cell Res*. 2017;27(1):109–118. doi:10.1038/cr.2016.151
34. Suh YJ, Park JH, Jeon JH, et al. Extrapleural solitary fibrous tumor of the thyroid gland: a case report and review of literature. *World J Clin Cases*. 2020;8(4):782–789. doi:10.12998/wjcc.v8.i4.782
35. Xiong J, Yang LY. Effects of alkaloid sinomenine on levels of IFN-γ, IL-1β, TNF-α and IL-6 in a rat renal allograft model. *Immunotherapy*. 2012;4(8):7. doi:10.2217/imt.12.80
36. De Vlaeminck Y, Bonelli S, Awad RM, et al. Targeting neuropilin-1 with nanobodies reduces colorectal carcinoma development. *Cancers*. 2020;12(12):3582. doi:10.3390/cancers12123582
37. Wang T, Wang D, Yu H, et al. Intracellularly acid-switchable multifunctional micelles for combinational photo/chemotherapy of the drug-resistant tumor. *ACS nano*. 2016;10(3):3496–3508. doi:10.1021/acsnano.5b07706
38. You Y, Xu Z, Chen Y. Doxorubicin conjugated with a trastuzumab epitope and an MMP-2 sensitive peptide linker for the treatment of HER2-positive breast cancer. *Drug Delivery*. 2018;25(1):448–460. doi:10.1080/10717544.2018.1435746